Geotechnical Aspects of Underground Construction in Soft Ground, Kusakabe, Fujita & Miyazaki (eds)

Stability of excavations in soft clay with floating self supported DMM wall

A. El Nahas & J. Takemura
Civil Engineering Department, Tokyo Institute of Technology, Japan

M. Kouda
Railway Research Institute, Japan

ABSTRACT: Centrifuge model tests were carried out in order to investigate the failure mechanism of excavations in soft clay using self supported walls made by deep mixing method. The wall was modeled using Aluminum and Acrylic plates and the external stability of the DMM wall was mainly studied. In-flight excavations were conducted until failure. The wall and ground deformations, pressures acting on the wall and pore water pressure in the soil were measured during excavations. It was found that adhesion mobilized on the wall surface had a significant effect on the stability. Sliding type failures were observed in the tests with wall height/width ratio less than 2 and the failure suddenly took place without showing marked pre-failure deformation.

1. INTRODUCTION

Self supported wall (SSW) made by deep mixing method (DMM) is a relatively recent application for excavations in soft clay. Although this type of wall tend to be rather expensive compared with common flexible braced walls (e.g. sheet pile walls), it can be economically feasible for large area shallow excavation in soft soil where no good bearing strata for ground anchors. Mechanical behaviour of the self supported wall in soft soil is totally different from that of the traditional self-supported gravity walls which are usually constructed on a good foundation.

As the stiffness of soil treated with DMM is far higher than that of the untreated soil, the external and internal stability were evaluated separately in the design of the wall. Hence previous studies on this type of wall are also divided into the two subjects, i.e., internal and external stability. Kitazume et al. (1996) and Babasaki et al. (1998) investigated the effects of reinforcement in DMM on the internal stability aiming at the reduction of the cross sectional area of the wall. Shiomi et al. (1996) and Chen et al. (1996) studied external stability of the wall floating in clay through an actual construction and a centrifuge model test respectively. Although some studies have been conducted, classic design methods of traditional self-supported walls are adopted for this wall type.

This paper describes the results of three centrifuge model tests on the excavation in normally consolidated clay using self-supported DMM walls floating in the clay. Effects of the wall dimensions and mobilized adhesion on the wall surfaces on the failure mechanism and earth pressures on the wall are discussed.

2. CENTRIFUGE MODEL TESTS

2.1 Test systems and conditions

TIT Mark III Centrifuge, in-flight excavator and steel made model container with transparent acrylic window were used in the tests. Their detail and specification are given by Kimura, et al. (1993) and Takemura, et al. (1999).

Test setup used in this study is illustrated in Figure 1. Model ground prepared for the tests consisted of three layers, i.e., upper loose sand (γ_d=14.2kN/m^3 and 15mm thick) and lower dense sand (γ_{sat}=19.6kN/m^3 and 35mm thick) and normally consolidated clay (153mm thick) in between the two sand layers. Toyoura sand and kaolin clay were used for sand and clay layers respectively. Physical and mechanical properties of kaolin clay were listed in Table 1.

The model wall consisted of 2 aluminum plates and 3 acrylic plates as shown in Figures 2-3. The aluminum plates were instrumented with 6 and 5 pressure cells on the backside and front sides of the wall respectively. Three pressure cells were also installed on the tips of the aluminum plates and the central acrylic plate. Dimensions and surface roughness of the wall were parameters in the tests.

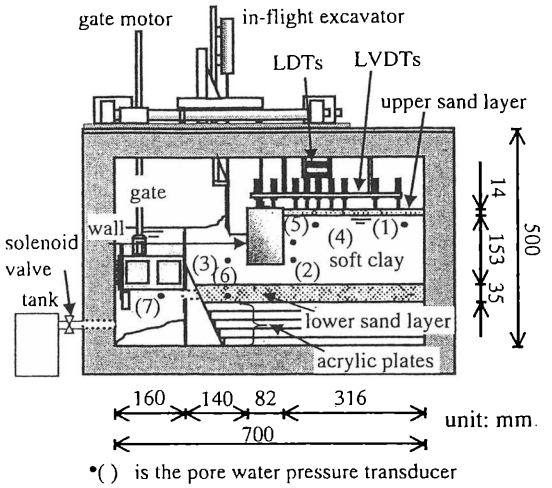

Figure 1. Test setup.

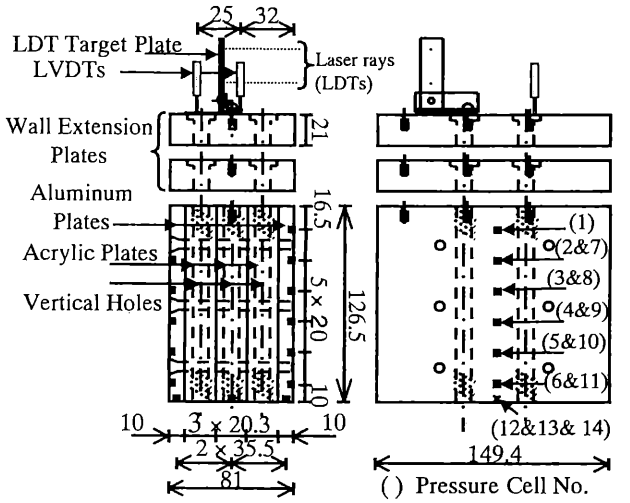

Figure 2. Model wall.

The height (H) and width (W) of the wall can be varied by putting top extension plates and changing the thickness of two non-instrumented acrylic plates respectively. The wall sides and bottom were covered with sandpaper sheets to create a rough surface. Table 2 shows the test conditions. Bulk density of the wall was 16.8 kN/m^3 slightly larger than that of the clay (γ_{sat}=15.6kN/m^3).

2.2 Test Procedure

In the preparation of the model setup, acrylic plates were first placed on the bottom of the container as spacers and the submerged dense sand layer was then made by compaction. Clay slurry remolded at water content 1.5 times the liquid limit was carefully deaired and poured into the container. Laboratory floor consolidation was conducted stepwise under the pressure of 15kPa. After completion of the consolidation, pore pressure transducers were

Table 1. Main physical and mechanical properties of the kaolin clay.

Liquid limit, w_L	Plastic limit, w_P	Specific gravity, G_s	K_0 for NC clay	c_{uc}/p' for NC clay
77.5%	30.3%	2.61	0.6	0.24

Table 2. Test conditions.

Test No.	H* (mm)	W (mm)	H/W	Surface condition
SSW-0	123	82	1.5	Smooth
SSW-3	123	82	1.5	Rough
SSW-4	163	82	2.0	Rough

*H is embedded height of the wall into soil layers

inserted in the clay. Subsequently brass rods giving rise to a surcharge pressure equal to the consolidation pressure on the lab floor in 70G field were placed at the clay surface and centrifugal consolidation was carried out at 70G to form a normally consolidated clay layer with strength increasing with depth.

On completion of the centrifugal consolidation, the centrifuge was once stopped. The brass rods were removed and then front window of the container was detached. A box shape steel cutter with width of 83mm was inserted into the clay at the location where the model wall was to be placed into the clay and the clay at the location was removed. The wall was then placed in the location. Greased membranes were put on the side surfaces of the wall to reduce the friction between the wall and the front window and back wall of the container. This membrane had a function to prevent the water flow from the side of the wall. Having placed the wall in the clay, the soil-retaining gate was installed in the container as shown in Figure1. Surface markers were placed on the clay surface and the front widow was attached to the container. Sand was then lain on the clay to form the upper sand layer. After installing LVDTs and laser displacement transducers (LDTs) and the excavator as shown in Figures 1& 2, the test setup was mounted on centrifuge and then the model ground was re-consolidated under 70G until excess pore pressure dissipated. During the consolidation, ground water table was kept at the level of the clay surface. Vertical stress profiles in terms of both total and effective stresses after the centrifugal consolidation are given in Figure 4 together with undrained compressive strength (c_{uc}) profile in the clay. Excavation was conducted step by step using the in-flight excavator (Kimura, et al.: 1993). In each step, soil was cut by about 10mm height (0.7m in prototype scale) from the front of the wall. The water level in the excavated area was lowered by draining water from the box to the

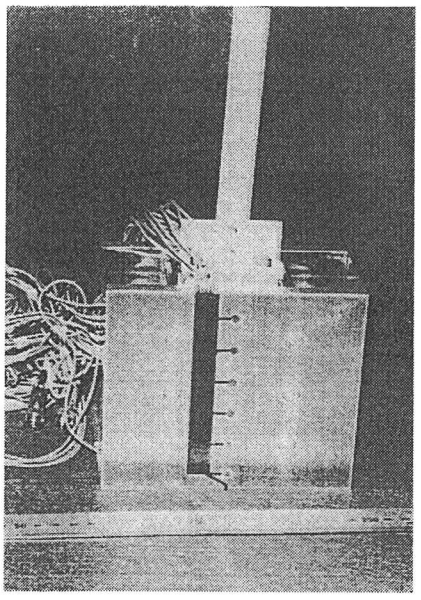

Figure 3. Photo of model wall.

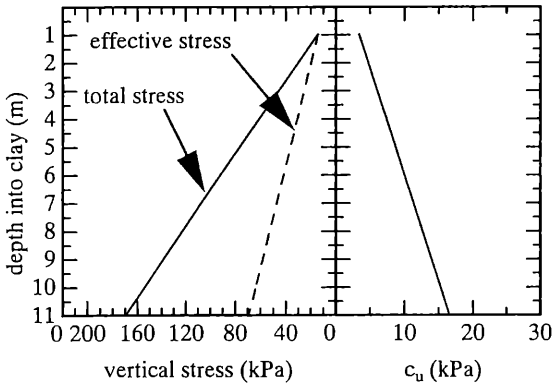

Figure 4. Profile of vertical stress and undrained compressive strength in clay.

drainage tank, so that it became the same as the excavation bottom. Excavation process, i.e. excavation depth (z_e) with time is shown in both model and prototype scale in Figure 5. Displacement of the wall and ground, pore water pressures and pressures on the front and back surfaces and base of the wall were measured during the excavation. Test results are all given in prototype scale in the following section.

3. TEST RESULTS AND DISCUSSION

3.1 Deformation of the wall and ground

Horizontal displacements of the wall top and bottom (dh_{top}& dh_{bot}) against excavation depth in Figure 6. Until some depth of excavation, only very small

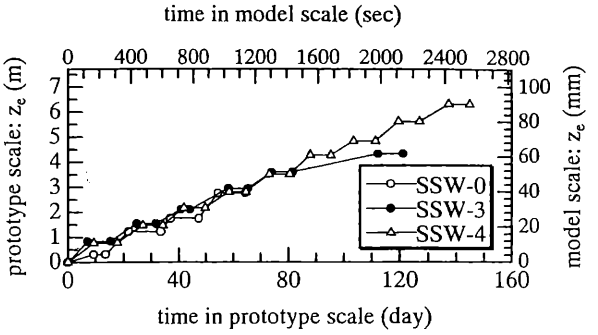

Figure 5. Process of excavation.

displacement was observed and then a sudden increase in the displacement took place without showing marked pre-failure deformation. From this figure failure excavation depth, $(z_e)_f$, was defined as the excavation depth at the intersection of the tangents for the z_e-*dh* relationships before and after sudden increase. In SSW-0, however, it was rather difficult to define the failure point using this definition because the excavation depth in one step was relatively larger than the failure depth. Hence the average of excavation depths before and after failure was taken as $(z_e)_f$ for SSW-0. The failure depth of each test is pointed with an arrow in the figure. It can be clearly seen from the figure that the roughness or adhesion of the wall surface and the increase of the wall height contribute to the increase of the excavation stability. A sudden increase of the horizontal displacement of the wall bottom occurred just before the wall showed a sudden increase of its tilting. The maximum measured tilting angles were less than 5 degrees. These imply that the wall first failed by sliding, thereafter some wall tilting towards the excavation side took place.

Figure 7 shows the variation of maximum settlement, S_{max}, of the retained soil behind the wall during excavation. S_{max} was small before the failure, and increased sharply at the failure point just like *dh* shown in Figure 6. This trend is more apparent in SSW-0&3. However, in SSW-4, the transition from the initial tangent to the failure was relatively gradual. In SSW-4, an increase of tilting can be seen before failure. This might be attributed to the gradual increase of the settlement.

Deformation of ground just after failure is shown in Figure 8. Marked horizontal displacement and smaller vertical one were observed in the wall, which clearly shows sliding type failure. On the active sides, the failed zone was bounded by a clear failure plane in all the cases. The failure plane in SSW-0 with smooth surface is steeper than that in SSW-3&4 with rough surface, resulting in wider failure zone in the latter than the former. The soils outside these planes and below the wall show no marked displacement even after failure. On the

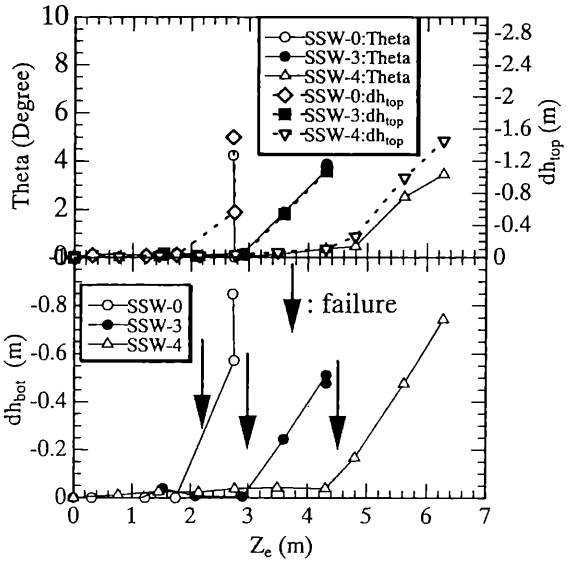

Figure 6. Variation of horizontal top and bottom displacements and tilting of wall during excavation.

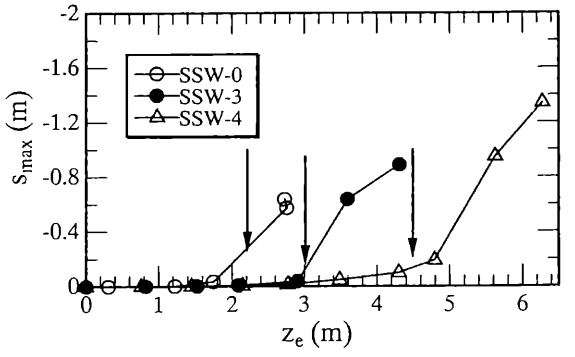

Figure 7. Variation of max. settlement behind the wall

passive sides, the soil deformed laterally with some vertical heave, without showing any clear failure planes.

Settlement distributions behind the wall observed just before and after failure are shown in Figure 9. From this figure, it can be also confirmed that only very small settlement took place even just before sudden collapse of the clay behind the wall. This may suggest that the crucial thing in the design of this type of wall is stability against failure not the deformation of the adjacent ground.

In order to estimate the failure excavation depth of each test, upper bound analysis was conducted using a simple sliding failure mechanism shown in Figure 10. The upper sand layer was assumed as a surcharge pressure q. Taking the strength anisotropy (Takemura, et al.: 1999) into account, compressive strength (c_{uc}) and extension strength (c_{ue}=0.6c_u) were used for the active and passive sides respectively in the analysis. Mobilized adhesion on the wall surface and base (c_w) were changed. The mobilized

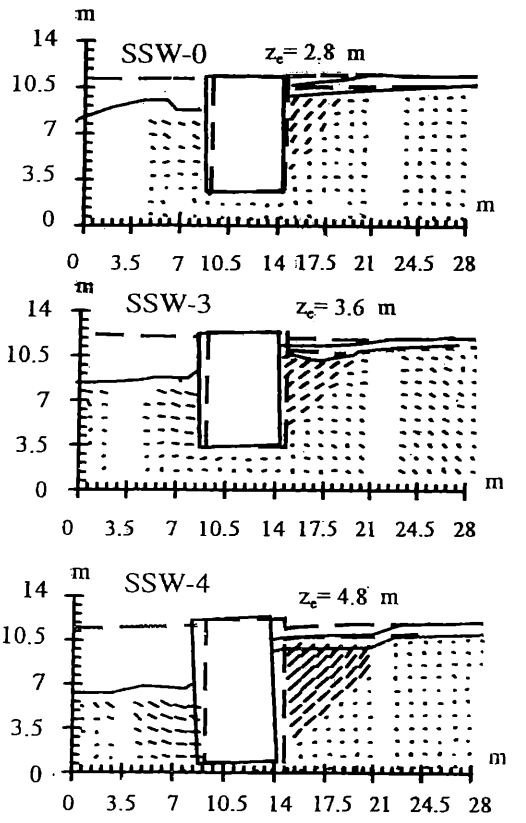

Figure 8. Observed deformation in the ground.

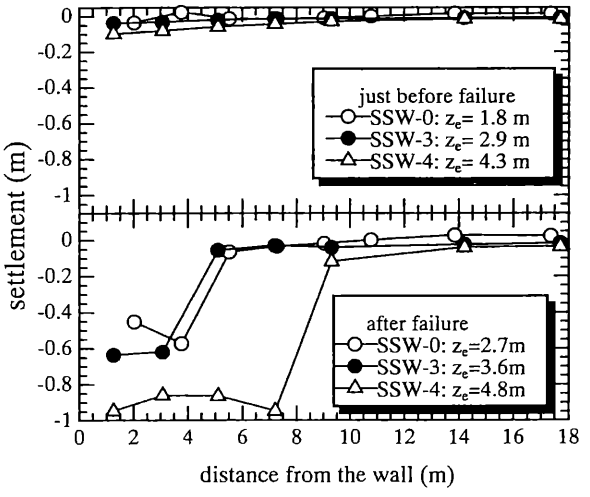

Figure 9. Settlement distribution behind the wall.

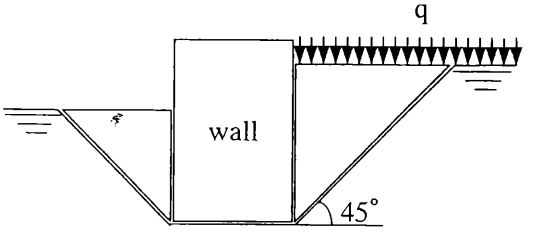

Figure 10. Failure mechanism used in the upper bound analysis.

adhesion for c_w/c_{uc}=0.8 corresponds to the average of compression and extension strengths. The calculated failure depths are shown in Table 3 together with test results. Normalized failure depths by the wall height are also given in the table. The calculated results show a significant effect of the surface adhesion on the stability. This compares well with the test results. The effect of the wall height estimated by the calculation is slightly less than that observed in the tests.

3.2 Pressures acting on the wall

Measured total earth pressure distributions on the wall before excavation and just before failure in SSW-3&4 are shown in Figure 11. The earth pressure at K_0 condition and active and passives ($p_{a,p}$) calculated using the following equation (Rowe, 1957) are also shown in the figure.

$$p_{a,p} = \gamma z + q \mp 2c_u\sqrt{1 + c_w / c_u} \qquad (1)$$

Strength anisotropy was also taken into account in this calculation. Although the differences of K_0 pressure and the calculated active pressure are small due to very low strength in NC clay, marked effects of the wall adhesion can also be seen in the calculated pressures. Observed earth pressures well compare with the calculated ones assuming c_w/c_{uc}=0.8 especially for the backside.

Figure 12 shows the measured contact pressures at the wall base before excavation and just before and after failure for SSW-3&4. The calculated values at the excavation depth just before failure shown in the figure were obtained from the moment equilibrium at the front wall base edge. Although some scattering was observed before excavation, it can be seen clearly that variations of contact pressure were very small from the initial condition until the failure in SSW-3 (H/B=3/2). While for SSW-4 with higher H/B (=2), quite large increase and decrease of the contact pressures were observed at the front and back wall base edges. The calculated values show that the adhesion can significantly reduce the stress concentration at the bottom edge. In SSW-3, the differences between the observed stress distribution under the wall base at failure and the calculated values, using c_w/c_{uc}=0.5, were so small. In SSW-4, the nearest prediction of the bearing stresses, to the observed values under the wall, was that calculated using c_w/c_{uc}=0.8. That means that, the mobilized adhesion in SSW-4 was larger than that mobilized in SSW-3. This result compares well with the comparison between the observed failure heights and the predicted values, using c_w/c_{uc}=0.5& 0.8 for SSW-3& 4, respectively as shown in Table 3.

Undrained strength of the ground at the depth of the wall base in SSW-4 was about 17kPa and the net

Table 3. Results of upper bound calculation of $(z_e)_f$.

Test case	Test result	c_w/c_u		
		0	0.5	0.8
SSW-0	2.2m (0.26)*	1.9m (0.23)	3.0m (0.36)	3.6m (0.43)
SSW-3	3.0m (0.36)			
SSW-4	4.5m (0.39)	2.3m (0.20)	3.5m (0.31)	4.1m (0.36)

*: number in bracket is $(z_e)_f/H$

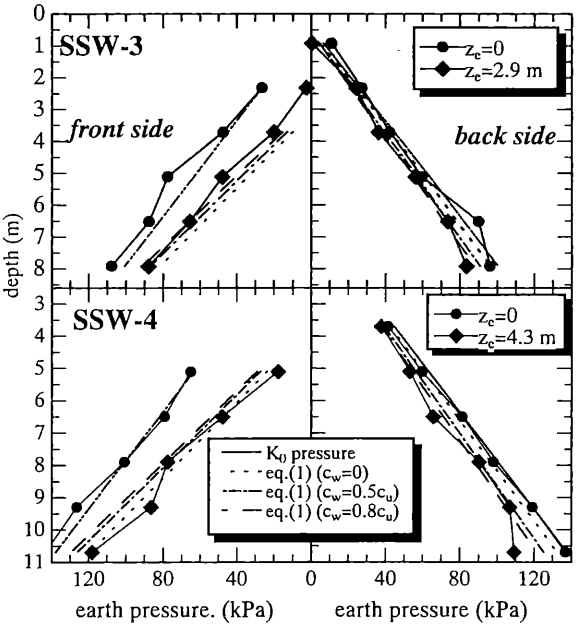

Figure 11. Total earth pressure on the wall surface.

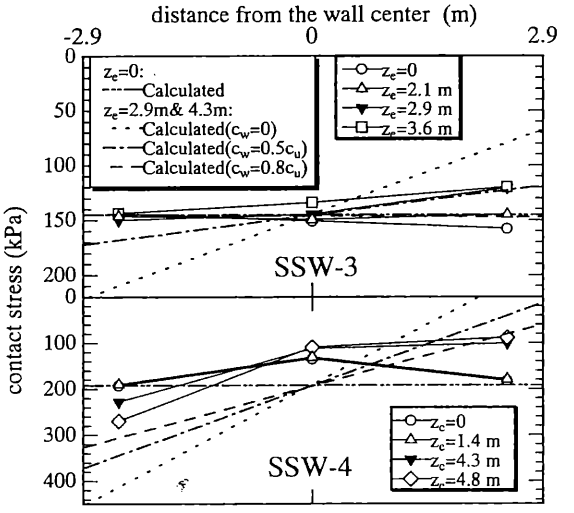

Figure 12. Contact pressures at wall base.

bearing pressure of the wall was about 90kPa. The increase of the calculated contact pressure with

c_w/c_{uc}=0.8 was almost the same as the net bearing capacity. From this it is considered that tilting failure due to overstressing the soil under the wall base may possibly dominate the failure mechanism for the wall with H/B larger than 2.

CONCLUSIONS

In this study the centrifuge model tests on excavations in soft normally consolidated clay using floating type self supported DMM walls were conducted. It was found that in this type of wall the failure suddenly took place without showing marked pre-failure deformation. This may suggest that in the design of this type of walls, the stability against failure is much more important than the deformation of the adjacent ground. It was also found that adhesion mobilized on the wall surface had a significant effect on the stability in decreasing active earth pressure, increasing passive pressure and increasing failure excavation depth. The adhesion may be attributed to the sliding type failure observed even in the wall with wall height/width ratio of 2.

REFERENCES

Babasaki, R et al. 1998. Design procedure for self-supporting earth retaining wall using Deep Mixing Method. *Centrifuge 98*, Tokyo, 1:673- 678.

Chen,X.L. et al. 1996. Design methods of cement-soil retaining wall. *Proc. 2nd Intl. Conf. Ground Improvement Geosystems-Grouting and Deep Mixing*, Tokyo, 475-480.

Kimura,T. et al. 1993. Stability of unsupported and supported vertical cuts in soft clay. *Proc. 11th Southeast Asian Geotechnical Conference*, Singapore, 61-70.

Kitazume, M. et al. 1996. Model tests on failure pattern of cement treated retaining wall, *Proc. 2nd Intl. Conf. Ground Improvement Geosystems-Grouting and Deep Mixing*, Tokyo, 509-514.

Rowe,P.W. 1957. Sheet pile walls in clay. *Inst. Civ. Engrgs*, 7: 629-654.

Shiomi,M. et al. 1996. Slope stability using the admixture method. *Proc. 2nd Intl. Conf. Ground Improvement Geosystems-Grouting and Deep Mixing*, Tokyo, 563-568.

Takemura, J. et al. 1999. Centrifuge model tests on double propped wall excavation in soft clay. *Soils and Foundations*, (to appear).